CHEMISTRY
A European Journal

A Journal of
ChemPubSoc Europe

Accepted Article

Title: Hexakis [60]Fullerene Adduct-Mediated Covalent Assembly of Ruthenium Nanoparticles and Their Catalytic Properties

Authors: Philippe Serp, Faqiang Leng, Iann C. Gerber, Pierre Lecante, Ahmed Bentaleb, Antonio Muñoz, Beatriz M. Illescas, Nazario Martín, Georgian Melinte, Ovidiu Ersen, Hervé Martinez, and M. Rosa Axet

To be cited as: *Chem. Eur. J.* 10.1002/chem.201701043

Link to VoR: http://dx.doi.org/10.1002/chem.201701043

Supported by
ACES

WILEY-VCH

10.1002/chem.201701043

WILEY-VCH

FULL PAPER

Hexakis [60]Fullerene Adduct-Mediated Covalent Assembly of Ruthenium Nanoparticles and Their Catalytic Properties

Faqiang Leng,[a],[b] Iann C. Gerber,[c] Pierre Lecante,[d] Ahmed Bentaleb,[e] Antonio Muñoz,[f] Beatriz M. Illescas,[f] Nazario Martín,[f],[g] Georgian Melinte,[h] Ovidiu Ersen,[h] Hervé Martinez,[i] M. Rosa Axet*[a],[b] and Philippe Serp*[a],[b]

Abstract: The $C_{66}(COOH)_{12}$ hexa-adduct has been successfully used as a building block to construct *via* carboxylate bridges 3D networks with very homogeneous sub-1.8 nm ruthenium nanoparticles. The obtained nanostructures are active in nitrobenzene selective hydrogenation.

Introduction

The synthesis of nanoparticle (NP) assemblies stabilized by functional molecules is a common research topic in nanoscience. The ability to control interparticle distances and positions in NP assemblies is one of the major challenges for the design and understanding of functional nanostructures. A combination of self- and directed-assembly processes, involving interparticle and externally applied forces, can be applied to produce the desired nanostructured materials. These processes usually involve non covalent interactions between NPs,[1] resulting in assemblies of poor mechanical stability, which can be detrimental to many applications. In order to obtain stable assemblies, and particularly metal NP assemblies, molecular linkers or mediators that can induce a covalent linking between the NPs have also been exploited.[1b, 2] The insertion of molecules with a large variety of size, shape, charge or electronic features allows to tune the metal interparticle interaction in NP assemblies bringing about novel functionalities. The properties of the resulting hybrid structures are not only interesting from a fundamental point of view, but are currently considered as technologically relevant, since they can address many cutting-edge applications such as plasmonic,[3] sensor,[4] or catalysis, where it has been shown that the proximity of the NPs may affect their catalytic performances and their stability.[5]

The use of C_{60} fullerene as a molecular linker is particularly attractive since: i) it is possible to produce bis-, tris-, tetrakis-, pentakis-, hexakis- and decakis-substituted C_{60} adducts,[6] paving the way to 1D, 2D or 3D assemblies of metallic NPs; and ii) the size of the [60]fullerene adduct is similar to the one of small NPs (1-1.5 nm). Only few reports in the literature deal with the assembly of metal NPs by [60]fullerene adducts, all of them with gold NPs.[7] The assembly of Au NPs by functionalized fullerenes through electrostatic interactions between negatively charged groups on Au NPs and positively charged piperazinyl groups on 1-(4-methyl)piperazinyl fullerene leads to 11.5-nm Au NPs assemblies with edge-to-edge interparticle distance of 1.14 ± 0.20 nm.[7a] A new organo-soluble C_{60} hexa-adduct bearing twelve thiocyanate functions has been used as a stabilizing/assembling agent to assemble homogeneous 3 nm Au NPs into apparently extended tridimensional networks.[7b] Hexakis-substituted [60]fullerene adducts have been recently identified as potential highly connective linkers for coordination polymer and metal–organic framework synthesis.[8]

Herein, we report the synthesis of $Ru@C_{66}(COOH)_{12}$ nanostructures, their characterization, and their use as catalysts.

Results and Discussion

The $Ru@C_{66}(COOH)_{12}$ nanostructures have been produced at room temperature from the reductive decomposition of [Ru(COD)(COT)] (COD= 1,5 cyclooctadiene, COT= 1,3,5-cyclooctatriene) by molecular H_2 in the presence of fullerenehexamalonic acid $C_{66}(COOH)_{12}$ (Scheme 1). The effect

[a] Dr. F. Leng, Dr. M. Rosa Axet, Pr. Dr. P. Serp
CNRS, LCC (Laboratoire de Chimie de Coordination)
composante ENSIACET, 4 allée Emile Monso, BP 44099, F-31030 Toulouse Cedex 4, France
E-mail: rosa.axet@lcc-toulouse.fr; philippe.serp@ensiacet.fr
[b] Dr. F. Leng, Dr. M. R. Axet, Pr. Dr. P. Serp
Université de Toulouse, UPS, INPT
F-31077 Toulouse Cedex 4, France
[c] Dr. I. C. Gerber
LPCNO, Université de Toulouse, CNRS, INSA, UPS
135 avenue de Rangueil, F-31077 Toulouse, France
[d] Dr. P. Lecante
Centre d'élaboration des matériaux et d'études structurales UPR CNRS 801
29 Rue Jeanne-Marvig, BP 4347, 31055 Toulouse, France Toulouse Cedex 4, France
[e] Dr. A. Bentaleb
Centre de Recherche Paul Pascal - CNRS University of Bordeaux
115 avenue Schweitzer 33600 Pessac, France
[f] Dr. A. Muñoz, Dr. B.M. Illescas, Pr. Dr. N. Martín
Departamento de Química Orgánica, Facultad de Ciencias Químicas, Universidad Complutense de Madrid, Madrid, Spain
23 rue du Loess BP43, 67034 Strasbourg cedex 2, France
[g] Pr. Dr. N. Martín
IMDEA-Nanoscience, Campus de Cantoblanco, Madrid, Spain.
[h] Dr. G. Melinte, Pr. Dr. O. Ersen
IPCMS, UMR 7504 Université de Strasbourg – CNRS, 23 rue du Loess, BP 43, 67034 Strasbourg Cedex 2, France.
[i] Pr. Dr. H. Martinez
IPREM CNRS UMR 5254, Helioparc Pau-Pyrénée, 2 Av du Pdt Angot, 64053 Pau Cedex, France

Supporting information for this article is given via a link at the end of the document.

10.1002/chem.201701043

FULL PAPER

of the solvent and the [Ru(COD)(COT)]/$C_{66}(COOH)_{12}$ ratio on the structure of the synthesized materials have been investigated.

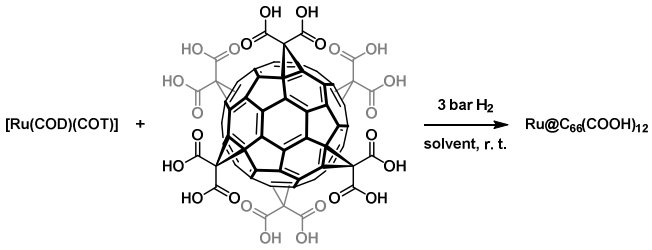

Scheme 1. Synthesis of $C_{66}(COOH)_{12}$-mediated covalent assembly of Ru NPs.

The produced nanostructures were characterized in detail using Transmission Electron Microscopy (TEM) and Electron Tomography together with Wide-Angle X-ray Scattering (WAXS), Small Angle X-ray Scattering (SAXS), Solid State NMR (SSNMR), X-ray Photoelectron Spectroscopy (XPS) and Attenuated Total Reflection Infrared spectroscopy (ATR-IR).

The effect of the solvent on the nanostructures was studied at a constant [Ru(COD)(COT)]/$C_{66}(COOH)_{12}$ ratio of 6/1. The solvents (THF, methanol and DMF) were chosen according to $C_{66}(COOH)_{12}$ solubility. Figure 1 shows the TEM images of the obtained materials. In all cases, objects with irregular shapes containing Ru NPs were observed. The Ru@$C_{66}(COOH)_{12}$ nanostructures synthesized in THF and MeOH (Fig. 1a and 1b and Fig. S1 in the SI) present the smallest Ru NPs, 1.23 ± 0.43 and 1.04 ± 0.30 nm, respectively. In the THF sample, the NPs are included in assemblies and no free NPs have been detected by TEM, contrarily to the samples prepared in MeOH and DMF. The synthesis carried out in DMF afforded less homogeneous and slightly larger Ru NPs (1.74 ± 0.87 nm, Fig. S1 in the ESI). THF was chosen as solvent as it produced homogeneous Ru NPs, which were all included in the assemblies. A series of experiments using Ru/$C_{66}(COOH)_{12}$ ratio from 6/1 to 50/1 were carried in THF out in order to investigate the effect of the Ru/ligand ratio on the nanostructures synthesised. The mean diameter of the Ru NPs increased slightly with increasing the Ru content (Table 1, and Fig. S2 in the ESI), while the nanostructures remained almost unchanged. The HREM images of Ru@$C_{66}(COOH)_{12}$ nanostructures 6/1 and 30/1 are depicted in Figure 2. Small Ru NPs are visible in both samples. The Ru NPs are well crystallized with crystal parameters corresponding to hexagonal close packed (*hcp)* Ru (Fig. 2b). EDX analyses have confirmed that the Ru@$C_{66}(COOH)_{12}$ nanostructures are composed of Ru and C (Fig. S3 in the ESI).

Table 1. Mean size diameters of Ru NPs with several Ru/$C_{66}(COOH)_{12}$ ratio.

Ru@$C_{66}(COOH)_{12}$	Ru loading[a] (%)	Nanoparticles mean size (nm)[b]
6/1	22.6	1.23 ± 0.43
12/1	40.7	1.54 ± 0.45
30/1	52.4	1.52 ± 0.44
50/1	nd	1.78 ± 0.79

[a]ICP analysis. [b]Mean values of size nanoparticle determined from TEM micrographs by considering at least 200 particles.

Ru@$C_{66}(COOH)_{12}$ samples synthesized in THF, sealed in Lindemann glass capillaries were also analysed by WAXS. The diffractograms of Ru@$C_{66}(COOH)_{12}$ 6/1, 12/1 and 30/1 are detailed in Fig. S4 in the ESI, and the pair-distribution functions (PDF) are displayed in Figure 3. The three diffractograms of Ru@$C_{66}(COOH)_{12}$ 6/1, 12/1 and 30/1 were very similar, and fully consistent with the presence of metallic *hcp* Ru.

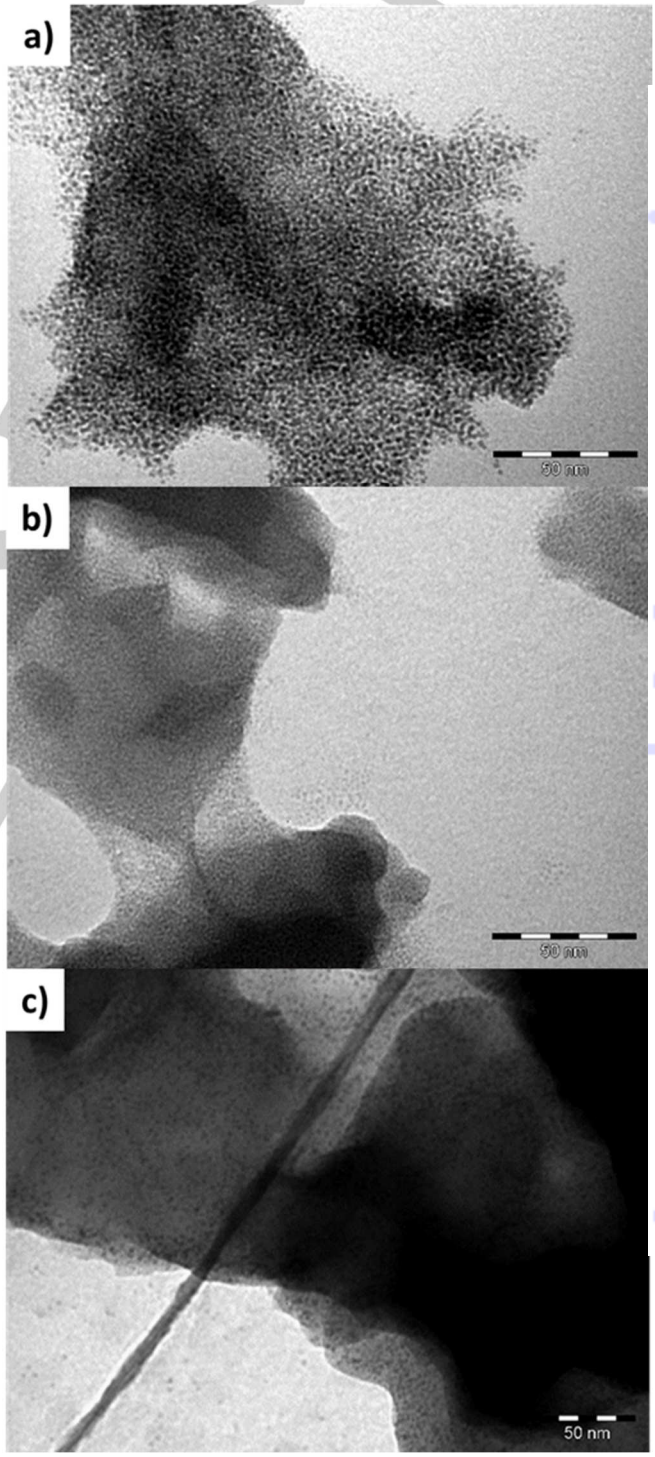

10.1002/chem.201701043

Figure 1. TEM micrographs of Ru@$C_{66}(COOH)_{12}$ nanostructures with Ru/$C_{66}(COOH)_{12}$ = 6/1 synthesized in different solvents: a) THF; b) MeOH; and c) DMF. (scale bars 50 nm).

The sharp peak signal at small angles is assigned to $C_{66}(COOH)_{12}$, since it is very similar to the feature of pure $C_{66}(COOH)_{12}$. After corrections and Fourier Transforms, the related PDF functions are also very similar (Fig. 3). The PDFs indicate that Ru NPs have a single size distribution and an average diameter close to 1.5 nm, in agreement with the TEM measurements.

SAXS analysis was performed on the Ru@$C_{66}(COOH)_{12}$ 12/1 nanostructure. The scattering intensity profile (Fig. 4) shows a global increase of the scattering intensity towards small q values, and is thus coherent with a system constituted of NPs. At higher q values, around q_{max} = 0.22Å^{-1}, we can observe a peak interpreted as a correlation distance between NPs. From the peak position, the correlation distance was found to be $2\pi/q_{max}$ = 2.85 nm. This value is considered as an average center to center distance between NPs in the superstructure and is coherent with a compact arrangement of the NPs, whose diameter is around 1.5 nm. Taking into account that the Ru NPs mean size diameter in Ru@$C_{66}(COOH)_{12}$ 12/1 nanostructure is 1.56 nm and the diameter of the $C_{66}(COOH)_{12}$ fullerene is 1.48 nm (calculated by DFT), the theoretical Ru NPs-Ru NPs distance is 3.04 nm, which correlates well with the distance found by SAXS (2.85 nm).

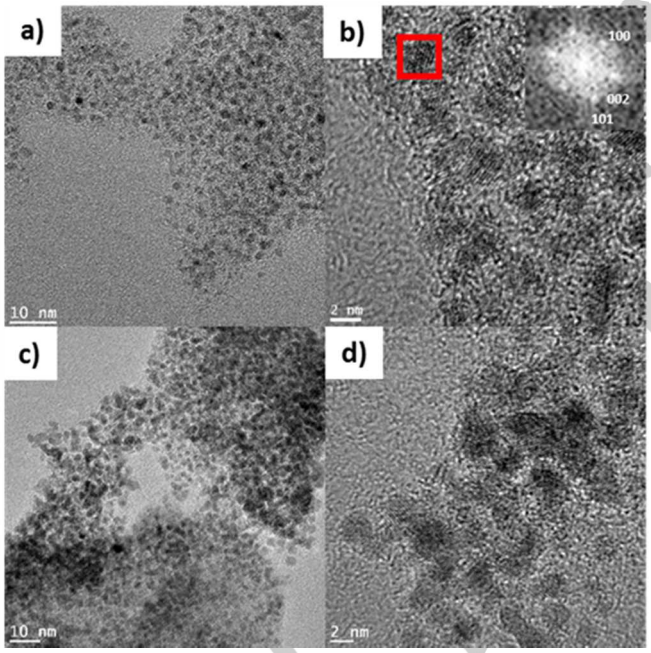

Figure 2. HREM micrographs of Ru@$C_{66}(COOH)_{12}$ nanostructures: a), b) Ru/$C_{66}(COOH)_{12}$ 6/1; inset: Fast Fourier Transform (FFT) with the corresponding orientation of the Ru lattice; and c), d) Ru/$C_{66}(COOH)_{12}$ 30/1.

To confirm the short range order between the ruthenium NPs, we performed an electron tomography analysis on a typical aggregate from the Ru@$C_{66}(COOH)_{12}$ 12/1 nanostructure. After 3D reconstruction from a tilt series of TEM images (Fig. 5, and video in SI), the 3D coordinates of all the NPs from the aggregate were determined and a pair distribution function was calculated by using a methodology previously described.[9] The distribution shows that the NPs do not present a long-range order, but as the well-defined peak appearing around 2.9 nm shows (Fig. 5d), a short-range one. This relatively broad peak is assigned to the first neighbour distance, as shown also in Fig. 5b. The electron tomography analyses are in a very good agreement with the SAXS results. XPS analysis of the Ru@$C_{66}(COOH)_{12}$ systems is inherently difficult because of the overlap of the C(1s) and Ru(3d) core levels, and the asymmetric nature of the Ru core level line shape.

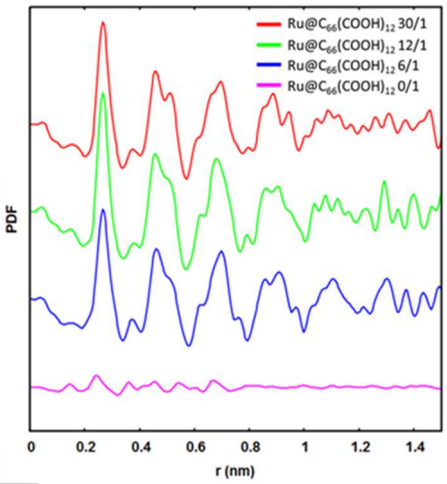

Figure 3. Pair-distribution functions of Ru@$C_{66}(COOH)_{12}$ 6/1, 12/1 and 30/1 nanostructures.

However, chemical state information may still be obtained from observing a combination of both the Ru(3d) and the less well-used Ru(3p) core levels, which presents a lower photoionization cross section. XPS analyses of Ru@$C_{66}(COOH)_{12}$ 12/1 are detailed in Table S1 and Fig. S5 in the ESI.The Ru 3d and C1s peaks have been deconvoluted into 8 peaks: O-C=O (288.5 eV), $C_{66}(COOH)_{12}$ sp^3-C (286.2 eV), C-C/C-H contamination (285.0 eV), $C_{66}(COOH)_{12}$ sp^2-C (284.4 eV), Ru $3d_{3/2}$ (280.5 eV) and Ru $3d_{5/2}$ (284.7 eV). O1s binding energy peaks are consistent with O=C-*O* (533 eV), *O*=C-O and/or C-*O*H (531.5 eV), and RuO_x (531.1 eV).

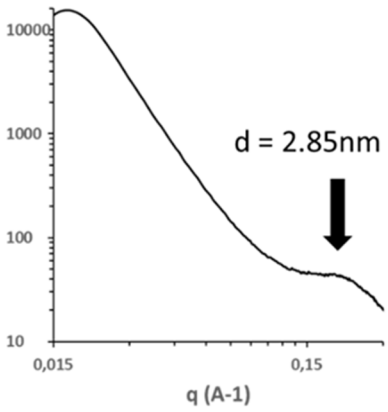

10.1002/chem.201701043

Figure 4. SAXS spectrum of Ru@$C_{66}(COOH)_{12}$ 12/1.

The Ru(3p) energy of 462.5 eV is consistent with the formation of RuO_x/Ru, and further supported by the Ru(3d) value of 280.5 eV.[10] The percentage of C and O found by XPS analyses (74.6% C, 22.2% O) was similar to the one expected for a Ru/$C_{66}(COOH)_{12}$ 12/1 ratio (70.3% C, 28.8% O). The coexistence of RuO_x and Ru(0) phases could be due to a coordination of carboxylate ligands from $C_{66}(COOH)_{12}$ on Ru NPs.[11]

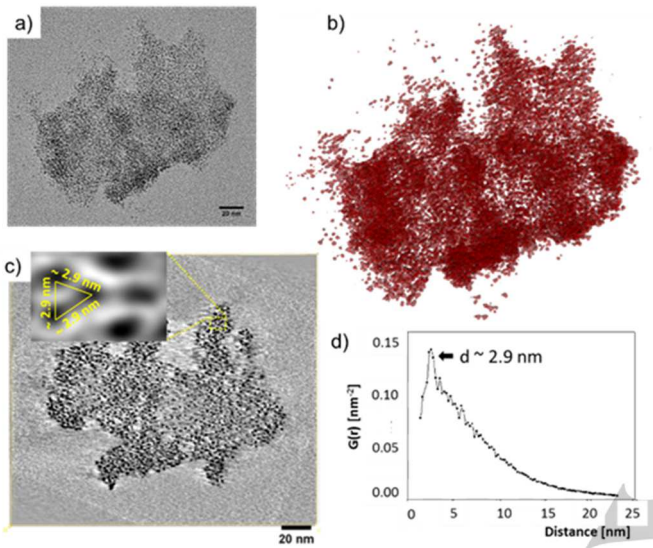

Figure 5. Electron tomography analysis of a representative aggregate from the Ru@$C_{66}(COOH)_{12}$ 12/1 sample. a) TEM image from the tilt series at 0° tilt. b) 3D model of the reconstructed volume showing the spatial distribution of all nanoparticles forming the aggregate. c) Typical longitudinal slice extracted from the reconstruction volume. The inserted image shows the distribution of a few NPs around a reference one. The repetitive distance is around 2.8 nm. d) Pair distribution function of the distances between NPs calculated from their 3D coordinates extracted from electron tomography data. Primary peak shows a short range order around 2.9 nm.

Solid-State NMR (SSNMR) and infrared spectroscopy, as well as DFT calculations were performed in order to get insight into the exact nature of the interaction between the Ru NPs and the $C_{66}(COOH)_{12}$ species. In $C_{66}(COOH)_{12}$, the first carboxylic group, $COOH_{(1)}$, of the malonic acid functional group behaves as an almost strong acid, whereas the second $COOH_{(2)}$ group is a weak acid with pK_2 of about 5.5. Thus, we can anticipate a different coordination of the $COOH_{(1)}$ and $COOH_{(2)}$ groups to the ruthenium center. ^{13}C-NMR SSNMR spectra of Ru@$C_{66}(COOH)_{12}$ 12/1 and 30/1 are displayed in Figure 6 together with the spectrum of the functionalized fullerene. The ^{13}C-NMR solid state NMR spectrum of $C_{66}(COOH)_{12}$ shows a peak at δ 69 ppm and a broad signal at 141-145 ppm attributed to the fullerene cage. In addition, a peak visible at δ 45 ppm is attributed to the quaternary carbon of the malonate moiety and a peak visible at δ 165 ppm to the carbon of the carbonyl moieties. The ^{13}C-NMR solid state NMR spectra of Ru@$C_{66}(COOH)_{12}$ 12/1 and 30/1 displayed the same number of peaks. The peaks at δ 69 ppm and 141-145 ppm attributed to the fullerene cage; remain unchanged with respect to the $C_{66}(COOH)_{12}$ compound in both samples, while the peaks attributed to the carboxylic groups shifted. The peak visible at δ 45 ppm attributed to the quaternary carbon upfield shifted of 20 ppm appearing at δ 25 ppm, and the peak attributed to the -COOH is splitted in two, with a downfield shifted to δ 185 ppm (see Figure 5b for CP-MAS ^{13}C-NMR), and still a contribution at 168 ppm. The shift of the peaks attributed to the -COOH moieties points out that $C_{66}(COOH)_{12}$ is coordinating to the Ru NPs thought these carbonyl moieties, probably in a carboxylate form. Also, the split of the peak of the carbonyl group indicates that the $COOH_{(1)}$ and $COOH_{(2)}$ groups do not present the same reactivity, which is probably related to the different acidity of the two acid functions of the malonic acid moieties. As infrared spectra can give supplementary information of the coordination mode of the fullerene ligands on the Ru NPs the ATR-IR spectra were recorded for $C_{66}(COOH)_{12}$ and Ru@$C_{66}(COOH)_{12}$ 6/1, 12/1 and 30/1 samples in the solid state (Fig. S6 in the ESI).

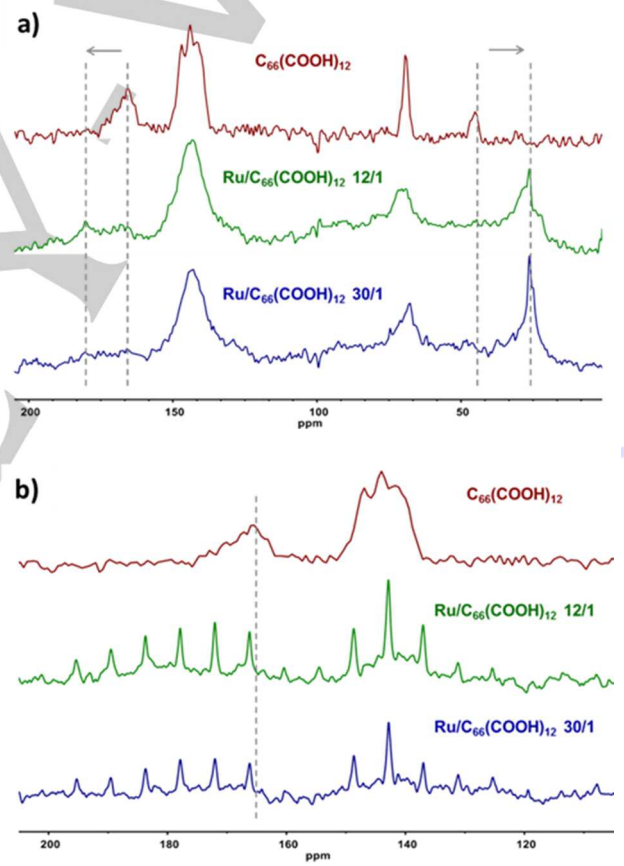

Figure 6. ^{13}C-NMR spectra of a) SSNMR and b) CP-MAS SSNMR of $C_{66}(COOH)_{12}$, Ru@$C_{66}(COOH)_{12}$ 12/1 and Ru@$C_{66}(COOH)_{12}$ 30/1.

The $C_{66}(COOH)_{12}$ ATR-IR spectrum show peaks at 2900, 1700, 1192, 830, 708, 540 and 524 cm^{-1}. The intense peaks at 2900 (COOH), 1700 (C=O), and 1192 (C-O) cm^{-1} are attributed to the -COOH moiety, while the other peaks are attributed to vibrations of the fullerene cage. Ru@$C_{66}(COOH)_{12}$ 6/1, 12/1 and 30/1 samples gave similar ATR-IR spectra. Peaks at 540 and 524 cm^{-1} attributed to the fullerene cage remained unchanged, while the

10.1002/chem.201701043

C=O vibration of the COOH group observed at 1700 cm^{-1}, present in the free ligand, is absent in the spectra of the Ru nanostructures. Two new peaks at 1555 and 1367 cm^{-1} were attributed to the C=O vibrations of a new COO-Ru species, confirming again the coordination of the fullerene through the carboxylate moieties. These data are in accordance with published values for Ru-carboxylate complexes.[12] A new peak at 1740 cm^{-1} corresponding to a C=O vibration, suggests that the $COOH_{(1)}$ and $COOH_{(2)}$ groups have not a similar reactivity. The peak at around 1900 cm^{-1} could be due the bond vibration of Ru-H species.[13],[14] or to partial decarbonylation of the $C_{66}(COOH)_{12}$ and further CO adsorption on the Ru particles. In order to get better insights of the molecular structure of the $Ru@C_{60}$ hybrids, Density Functional Theory (DFT) calculations have been performed.

To investigate the coordination modes of the functionalized C_{60} to Ru NPs, we have modelled the system using two functionalized C_{60} in interaction with a Ru_{13} cluster. As shown in Figure 7, the coordination mode implies 3 oxygens with a facet of the cluster consisting of 3 surface Ru atoms.

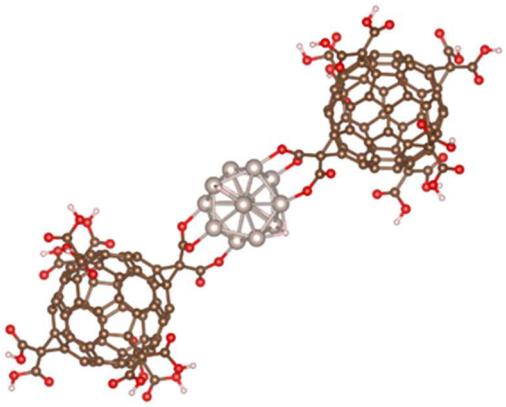

Figure 7. Optimized structure of the $C_{66}(COOH)_{12}$-Ru_{13}-$C_{66}(COOH)_{12}$ species.

This result confirms the different reactivity of the $COOH_{(1)}$ and $COOH_{(2)}$ groups, and explain the SSNMR and ATR-IR results. The Ru-O distances are typical of such systems with values ranging from 1.97 to 2.05 Å, in good agreement with a previous study on the interaction of Ru NPs with oxidized carbon nanotubes sidewalls.[15] Interestingly, as in a former study,[15] the migration of hydrides on the Ru cluster is spontaneous, resulting in the formation of carboxylate groups, with an energy gain of around 15 kcal/mol per H adsorbed. Globally the formation of this complex is highly favourable: -149 kcal/mol.

Finally, we performed a preliminary study on the catalytic activity of the $Ru@C_{66}(COOH)_{12}$ 6/1, 12/1 and 30/1 catalysts for nitrobenzene (NB) hydrogenation, and we compared their performances to the ones obtained with a [Ru(COD)(COT)]-$C_{66}(COOH)_{12}$ homogeneous mixture. NB hydrogenation was studied at 30 bar H_2 and 80°C in ethanol (see ESI for details).[16] We independently verified that under these experimental conditions, $C_{66}(COOH)_{12}$ was not active for this reaction. The results are presented on Table 2. The only reaction products were aniline (AN) and N-ethylaniline (AN-Et), which is formed from N-alkylation of AN due to reaction with the solvent, for all the catalysts except for $Ru@C_{66}(COOH)_{12}$ 30/1. For this latter catalyst, in a first step AN is produced, and in a second step AN is hydrogenated to cyclohexylamine (CA), which can also react with the solvent to produce N-ethylcyclohexylamine (CA-Et). Such a stepwise hydrogenation of NB, first to AN and then to CA has already been reported for $Ru@C_{60}$ catalysts.[16] The low metal loaded catalysts (Ru/C_{60} ratio ≤12) were found to be inactive for the hydrogenation of the aromatic ring, and AN was produced with selectivity >80%. An explanation could be that, since complete conversion of NB is not reached with these samples due to the low Ru loading, the AN hydrogenation did not proceed. While the initial activity of the $Ru@C_{66}(COOH)_{12}$ systems is relatively high (up to TOF = 89 h^{-1}), it decreases to reach a value of approximately 30 h^{-1} in all Ru NPs catalysts. In contrast, the activity of the [Ru(COD)(COT)]-$C_{66}(COOH)_{12}$ homogeneous catalyst slightly increases with reaction time with a TOF of 18 h^{-1} at 1h to reach 27 h^{-1} at 4h. This behavior points out that probably the [Ru(COD)(COT)] complex decomposes during catalysis to give Ru NPs as it can be easily decomposed in the presence of H_2. Indeed, a black solid was collected after reaction, pointing towards a decomposition reaction of the [Ru(COD)(COT)] complex during catalysis. However, no metallic NPs have been observed on this material by TEM; although the formation of small clusters cannot be excluded (Figure S7 in the ESI) After reaction, the size of the Ru NPs in $Ru@C_{66}(COOH)_{12}$ samples was not significantly changed (Figure S7 in the ESI).

Table 2. Activity and selectivity for the nitrobenzene hydrogenation for the $Ru@C_{66}(COOH)_{12}$ and [Ru(COD)(COT)]-$C_{66}(COOH)_{12}$ catalysts.

Catalyst	[Ru] (mM)	TOF[a] (h^{-1})	Conversion[b] (%)	Selectivity[b] (%)			
				AN	*AN-Et*	*CA*	*CA-Et*
[Ru(COD)(COT)]-$C_{66}(COOH)_{12}$ 12/1	0.66	18	64	89	10	---	---
$Ru@C_{66}(COOH)_{12}$ 6/1	0.37	89	88	84	16	---	---
$Ru@C_{66}(COOH)_{12}$ 12/1	0.66	62	97	85	15	---	---
$Ru@C_{66}(COOH)_{12}$ 30/1	0.86	51 (123)[c]	100	90	10	80[d]	20[d]

Reaction conditions: 5 mg of catalyst, 500 mg (4.06 mmol) of NB, 200 mg (1.1 mmol) of dodecane (internal standard), 30 bar H_2, 80 °C, 30 mL EtOH. [a] TOFs calculated after 1 hour reaction for nitrobenzene hydrogenation to aniline. [b] Determined by GC-MS using the internal standard technique at 60% conversion.[c] Value in parentheses corresponds to the TOF calculated after 1 hour reaction for aniline hydrogenation to cyclohexylamine. [d] Determined by GC-MS at 100% conversion of AN.

Conclusions

Hexasubstituted fullerene $C_{66}(COOH)_{12}$ is able to stabilize small Ru NPs (1.23-1.78 nm) synthesised under mild reaction conditions from [Ru(COD)(COT)]. SAXS and electron tomography analyses show that Ru NPs are organized, displaying a Ru NPs distance of 2.85 nm in the case of $Ru@C_{66}(COOH)_{12}$ 12/1 synthesized in THF. TEM analyses together with WAXS measurements corroborate that the Ru NPs are well crystallized and display an *hcp* structure. Furthermore, IR, SSNMR and XPS point out that the substituted fullerene coordinates to the Ru NPs *via* carboxylate groups, which is corroborate by DFT calculations. The $Ru@C_{66}(COOH)_{12}$ materials display high selectivity and activity in nitrobenzene hydrogenation. Finally, it is important to stress that such a methodology can be apply to a family of materials that could find applications in many other fields than catalysis.

Experimental Section

General Methods

All operations were carried out under argon atmosphere using standard Schlenk techniques or in an MBraun glovebox. Solvents were purified by standard methods or by an MBraun SPS-800 solvent purification system. [Ru(COD)(COT)] was purchased from Nanomeps Toulouse, fullerene C_{60} (99.5%), diethyl malonate(99%), carbon tetrabromide (CBr_4 99%), 1,8-diazabicyclo[5.4.0]undec-7-ene (DBU 98%), Amberlite IR-120 hydrogen form from Sigma-Aldrich, CO and H_2 from Air Liquid. All these reactants were used as received. The ruthenium content in the products was measured by inductively coupled plasma optical emission spectroscopy (ICP-OES) performed at the LCC with a Thermo Scientific ICAP 6300 instrument. Solid state NMR (MAS-NMR) with and without ^{1}H-^{13}C cross polarization (CP) were performed at the LCC on a Bruker Avance 400WB instrument equipped with a 4 mm probe with the sample rotation frequency being set at 12 kHz, unless otherwise indicated. Measurements were carried out in a 4 mm ZrO_2 rotor. Liquid NMR spectra were obtained on Bruker Fourier 300 systems using $CDCl_3$/*d*-acetone as solvent, TMS as internal standard, with proton and carbon resonances at 300 and 75 MHz, respectively. ATR-IR spectra were recorded on a Perkin-Elmer GX2000 spectrometer installed in a glovebox, in the range 4000-400 cm^{-1}. GC-MS analyses were performed in a PerkinElmer Autosystem GC equipped with an Elite-5MS Capillary Column (30 m × 0.25 mm × 0.25 µm) coupled to a Turbo Mass mass spectrometer. Hydrogenation reactions were performed in Top Industry high pressure and temperature stainless steel autoclave with a controlling system.

TEM analyses

TEM and HRTEM analyses were performed at the "Centre de microcaracterisation Raimond Castaing, UMS 3623, Toulouse" by using a JEOL JEM 1011 CX-T electron microscope operating at 100 kV with a point resolution of 4.5 Å and a JEOL JEM 1400 electron microscope operating at 120 kv. The high resolution analyses were conduct using a JEOL JEM 2100F equipped with a Field Emission Gun (FEG) operating at 200 kV with a point resolution of 2.3 Å and a JEOL JEM-ARM200F Cold FEG operating at 200 kV with a point resolution of >1.9 Å. The particles size distribution was made through a manual measurement of enlarged micrographs from different areas of the TEM grid (at least 200 particles). Other TEM micrographs were acquired with a JEOL 2100F S/TEM microscope equipped with a FEG operating at 200 kV, a spherical aberration probe corrector and a GATAN Tridiem energy filter. Experimental data for tomography were acquired by means of a JEOL 2100F transmission electron microscope with a field emission gun operating at 200 kV. The tilt series of TEM bight field images were recorded with a 2048 x 2048 pixel cooled CCD detector having a pixel size of about 0.25 nm and a 1 s exposure time for each record. The angular interval sampled during the acquisition was between 68 and -70°, with a tilt increment given by a 1.7°, giving a total of 82 images. The volume reconstructions were computed using the simultaneous iterative reconstruction techniques (SIRT) implemented in the Tomo3d.[17] Visualization and quantitative analysis of the calculated volumes were carried out using Slicer and ImageJ Software.

DFT Calculations

DFT calculations were carried out using the Vienna ab initio simulation package VASP.[18] The code uses the full-potential projector augmented wave (PAW) framework.[19] Exchange-correlation effects have been approximated using the PBE functional[20] and applied in spin-polarized calculations. A kinetic-energy cutoff of 400 eV was found to be sufficient to achieve a total-energy convergence within several meV, considering a k-point sampling in Gamma-point only calculations for isolated molecules and complexes, in conjunction with a Gaussian smearing with a width of 0.05 eV. All the atoms were fully relaxed until forces on individual atoms were smaller than 0.01 eV/Å. Calculation cells for isolated molecules and complexes were (25x26x27) $Å^3$, to avoid spurious interactions between periodic images. Figures of the different geometries were produced thanks to the 3D visualization program VESTA.[21]

SAXS, WAXS and XPS analyses

The samples were characterized by small-angle X-ray scattering (SAXS) on a Nanostar (Bruker Co.), equipped with a Siemens Copper anode (40kV 35mA). The apparatus is equipped with two crossed Goebel mirrors in order to select the CuKα wavelength (0.154 nm) and produces a parallel beam, the final collimation being adjusted with a three-pinhole setup (with a 300 µm diameter for pinhole-2 setting the beam size). SAXS patterns were acquired using a 22 × 22 cm 2D gas detector HiStar from Bruker Co., positioned at a distance D of the sample. Silver behenate was used as a calibration standard, yielding D = 1.06 m. The scattering wave vector range used was 0.1–2.0 nm^{-1}. Wide Angle X-ray Scattering measurements were performed at CEMES on a diffractometer dedicated to Pair Distribution Function (PDF) analysis: graphite-monochromatized Molybdenum radiation (0.07169 nm), solid state detection and low background setup. Samples were sealed in Lindemann glass capillaries (diameter 1.5mm) to avoid any oxidation after filling in a glove box. For all samples data were collected on an extended angular range (129 degrees in 2theta) with counting times of typically 150s for each of the 457 data points, thus allowing for PDF analysis. Classic corrections (polarization and absorption in cylindrical geometry) were applied before reduction and Fourier transform. The samples were also analyzed by X-ray photoelectron spectroscopy (XPS) using a VG Escalab MKII spectrophotometer, which operated with a non monochromatized Mg K source (1253.6 eV).

Synthesis of fullerene derivatives

$C_{66}(COOH)_{12}$ was synthesized by reaction of an excess of NaH with the T_h-hexa-adducts diethyl malonate fullerene $C_{66}(COOEt)_{12}$,[22] which was synthesized by nucleophilic cyclopropanation of fullerene C_{60} with diethyl bromo-malonate using a previously described procedure.[23]

10.1002/chem.201701043

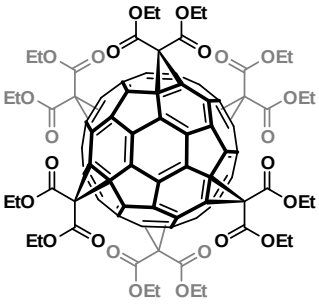

$C_{66}(COOEt)_{12}$. CBr_4 (22.8g, 69.5 mmol), diethyl malonate (1.104 g, 6.9 mmol) and DBU (2.1 g, 13.8 mmol) were dissolved in dry toluene (500 ml) and the solution was successively added to a fullerene C_{60} solution (500 mg, 0.7 mmol). The reaction was allowed to react during 4 days. The reaction crude was purified by flash chromatography using a toluene/ethyl acetate mixture. The product was isolated as a yellow solid (580 mg, 49% yield). ^{1}H-NMR ($CDCl_3$, 300 MHz, ppm): δ= 4.33 (q, *J* = 7.14 Hz, 24H, -C*H*$_2$-), 1.33 (t, *J* = 7.11 Hz, 36H, -C*H*$_3$); ^{13}C-NMR ($CDCl_3$, 75 MHz, ppm): δ= 164 (*C*=O), 146 (sp^2-*C* C_{60}), 141 (sp^2-*C* C_{60}), 69.2 (sp^3-*C* C_{60}), 62.9 (-*C*H$_2$-), 45.5 (tert-*C*), 14.2 (-*C*H$_3$).

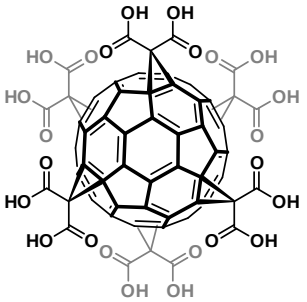

$C_{66}(COOH)_{12}$. $C_{66}(COOEt)_{12}$ (200 mg, 0.119 mmol) was dissolved in 50 mL of toluene, and NaH (57.2 mg, 2.38 mmol) was slowly added to the solution. The resulting mixture was stirred 3h at 75 °C. The reaction mixture was centrifuged, after the precipitate was washed with toluene three times (10 ml). Afterwards the crude was dissolved in distilled water and the solution passed through a resin (Amberlite IR-120 hydrogen form). The water was evaporated to afford a yellow-brown solid (127 mg, 80% yield).C^{13}-NMR (*d*-acetone, 75 MHz, ppm): δ= 164.7 (*C*=O), 146.3 (sp^2-*C* C_{60}), 142.5 (sp^2-*C* C_{60}), 70.4 (sp^3-*C* C_{60}), 47.7 (tert-*C*). IR (ATR): *v* 2900 (COOH), 1700 (C=O), 1192 (C-O), 830, 708, 540 (-C_{60}), 524 (-C_{60}). Anal. Calcd. for $C_{78}O_{24}H_{12}$ (1332 g/mol): C, 70.3; H, 0.01. Found: C, 60; H, 1.8.

Synthesis of Ru@$C_{66}(COOH)_{12}$ nanostructures

In a typical experiment [Ru(COD)(COT)] complex was introduced in a Fisher-Porter bottle, and a solution of $C_{66}(COOH)_{12}$ in the desired solvent was then introduced in the reactor. The resulting solution was stirred for 30 min at room temperature, after which the bottle was pressurized with 3 bar of H_2. The solution, which turned black after few minutes of reaction, was stirred overnight at room temperature. After this period of time, the H_2 pressure was released and the volume of solvent was reduced under vacuum. Pentane was then added to the colloidal suspension to precipitate the Ru@$C_{66}(COOH)_{12}$ nanostructures. After filtration under argon with a cannula, the black solid powder was washed twice with pentane and filtrated again before drying under vacuum overnight. For each ratio studied, the quantities of reactants are detailed hereafter:

Ru@$C_{66}(COOH)_{12}$ 6/1: 100 mg (0.32 mmol) of [Ru(COD)(COT)]; 70.4 mg (0.053 mmol) of $C_{66}(COOH)_{12}$ and 150 mL of THF. Yield: 82 mg. Ru: 22.6%

Ru@$C_{66}(COOH)_{12}$ 12/1: 113.5 mg (0.36 mmol) of [Ru(COD)(COT)]; 45 mg (0.035 mmol) of $C_{66}(COOH)_{12}$ and 100 mL of THF. Yield: 69mg. Ru: 40.7%

Ru@$C_{66}(COOH)_{12}$ 30/1: 282 mg (0.90 mmol) of [Ru(COD)(COT)]; 40 mg (0.033 mmol) of $C_{66}(COOH)_{12}$ and 90 mL of THF. Yield: 116 mg. Ru: 52.4%.

Ru@$C_{66}(COOH)_{12}$ 50/1: 41.7 mg (0.13 mmol) of [Ru(COD)(COT)]; 3.5 mg (0.003 mmol) of $C_{66}(COOH)_{12}$ and 10 mL of THF. Yield: 5 mg.

General procedure for the hydrogenation of nitrobenzene

Hydrogenation reactions were performed in a Top Industry high pressure and temperature stainless steel autoclave with a controlling system. In a typical experiment, the autoclave was purged by three vacuum/argon cycles. The mixture of 5 mg of Ru@$C_{66}(COOH)_{12}$ catalysts (for [Ru(COD)(COT)]-$C_{66}(COOH)_{12}$ 12/1 homogeneous catalyst: 6.2 mg of [Ru(COD)(COT)] and 2.4 mg of $C_{66}(COOH)_{12}$), dodecane (as internal standard, 200 mg, 1.1 mmol) and nitrobenzene (500 mg, 4.06 mmol) in 30 mL of ethanol was prepared in a glovebox, ultrasonicated for 5 min and then transferred into a high-pressure autoclave under argon atmosphere. The autoclave was heated to 80°C and pressurized with 30 bar of H_2; the stirring rate was fixed at 1000 rpm. Samples of the reaction mixture were taken periodically and then analyzed by GC-MS. Quantitative analysis of reaction mixtures was performed via GC-MS using calibration solutions of commercially available products.

Acknowledgements

This work was supported by the Centre National de la Recherche Scientifique (CNRS), which we gratefully acknowledge. The authors acknowledge financial support from the program of China Scholarships Council (CSC) for F. L. grant. I.C. Gerber also acknowledges the Calcul en Midi-Pyrénées initiative-CALMIP (Project p0812) for allocations of computer time and GENCI-IDRIS and CINES through the project x2016096649. We also thank the European Research Council (ERC-320441-Chirallcarbon), and the CAM FOTOCARBON project S20.

Keywords: Ru • Fullerenes • C_{60} • Nanomaterials • Polymers

[1] a) Y. Min, M. Akbulut, K. Kristiansen, Y. Golan and J. Israelachvili, *Nat. Mater* **2008**, *7*, 527-538; b) M.-A. Neouze, *J. Mater. Sci.* **2013**, *48*, 7321-7349.

[2] a) S. I. Lim and C.-J. Zhong, *Acc. Chem. Res.* **2009**, *42*, 798-808; b) R. Schreiber, J. Do, E.-M. Roller, T. Zhang, V. J. Schuller, P. C. Nickels, J. Feldmann and T. Liedl, *Nat. Nano* **2014**, *9*, 74-78.

[3] Y. Zhang, Q. Liu, H. Mundoor, Y. Yuan and I. I. Smalyukh, *ACS Nano* **2015**, *9*, 3097-3108.

[4] a) J. B. Edel, A. A. Kornyshev and M. Urbakh, *ACS Nano* **2013**, *7*, 9526-9532; b) Z. Nie, A. Petukhova and E. Kumacheva, *Nat. Nano* **2010**, *5*, 15-25.

[5] a) P. Munnik, P. E. de Jongh and K. P. de Jong, *J. Am. Chem. Soc.* **2014**, *136*, 7333-7340; b) G. Prieto, J. D. Meeldijk, K. P. de Jong and P. E. de Jongh, *J. Catal.* **2013**, *303*, 31-40; c) G. Prieto, M. Shakeri, K. P. de Jong and P. E. de Jongh, *ACS Nano* **2014**, *8*, 2522-2531; d) G. Prieto, J. Zečević, H. Friedrich, K. P. de Jong and P. E. de Jongh, *Nat. Mater.* **2013**, *12*, 34-39.

[6] W. Yan, S. M. Seifermann, P. Pierrat and S. Brase, *Org. Biomol. Chem.* **2015**, *13*, 25-54.

[7] a) I. I. S. Lim, J. Ouyang, J. Luo, L. Wang, S. Zhou and C.-J. Zhong, *Chem. Mater.* **2005**, *17*, 6528-6531; b) G. Rousseau, C. Lavenn, L. Cardenas, S. Loridant, Y. Wang, U. Hahn, J.-F. Nierengarten and A. Demessence, *Chem. Commun.* **2015**, *51*, 6730-6733; c) H. Fujihara and H. Nakai, *Langmuir* **2001**, *17*, 6393-6395; d) P. Sudeep, B. I. Ipe, K. G. Thomas, M. George, S. Barazzouk, S. Hotchandani and P. V. Kamat, *Nano Letters* **2002**, *2*, 29-35; e) Y.-S. Shon and H. Choo, *Chem. Commun.* **2002**, 2560-2561; f) F. Lu, S. Xiao, Y. Li, Y. Song, H. Liu, H. Li, J. Zhuang, Y. Liu, L. Gan and D. Zhu, *Inorg. Chem. Commun.* **2004**, *7*, 960-962; g) M. Geng, Y. Zhang, Q. Huang, B. Zhang, Q. Li, W. Li and J. Li, *Carbon* **2010**, *48*, 3570-3574; h) P. Zhang, J. Li, D. Liu, Y. Qin, Z.-X. Guo and D. Zhu, *Langmuir* **2004**, *20*, 1466-1472; i) I.-I. S. Lim, Y. Pan, D. Mott, J. Ouyang, P. N. Njoki, J. Luo, S. Zhou and C.-J. Zhong, *Langmuir* **2007**, *23*, 10715-10724; j) A. Hirsch and O. Vostrowsky, *Eur. J. Org. Chem.* **2001**, *2001*, 829-848; k) P. Pierrat, S. Vanderheiden, T. Muller and S. Brase, *Chem. Commun.* **2009**, 1748-1750.

[8] A. Kraft, P. Roth, D. Schmidt, J. Stangl, K. Müller-Buschbaum and F. Beuerle, *Chem. Eur. J.* **2016**, *22*, 5982-5987.

[9] I. Florea, A. Demortière, C. Petit, H. Bulou, C. Hirlimann and O. Ersen, *ACS Nano* **2012**, *6*, 2574-2581.

[10] S. Iqbal, S. A. Kondrat, D. R. Jones, D. C. Schoenmakers, J. K. Edwards, L. Lu, B. R. Yeo, P. P. Wells, E. K. Gibson, D. J. Morgan, C. J. Kiely and G. J. Hutchings, *ACS Catal.* **2015**, *5*, 5047-5059.

[11] J. V. Rojas, M. Toro-Gonzalez, M. C. Molina-Higgins and C. E. Castano, *Mater. Sci. Eng., B* **2016**, *205*, 28-35.

[12] T. Stephenson and G. Wilkinson, *Journal of Inorganic and Nuclear Chemistry* **1966**, *28*, 2285-2291.

[13] N. A. Jasim, R. N. Perutz, S. P. Foxon and P. H. Walton, *Journal of the Chemical Society, Dalton Transactions* **2001**, 1676-1685.

[14] X. Wang and L. Andrews, *The Journal of Physical Chemistry A* **2008**, *113*, 551-563.

[15] B. F. Machado, M. Oubenali, M. R. Axet, T. T. Nguyen, M. Tunckol, M. Girleanu, O. Ersen, I. C. Gerber and P. Serp, *Journal of Catalysis* **2014**, *309*, 185-198.

[16] F. Leng, I. C. Gerber, P. Lecante, S. Moldovan, M. Girleanu, M. R. Axet and P. Serp, *ACS Catal.* **2016**, *6*, 6018-6024.

[17] J.-I. Agulleiro and J.-J. Fernandez, *J. Struct. Biol.* **2015**, *189*, 147-152.

[18] a) G. Kresse and J. Furthmüller, *Comput. Mater. Sci.* **1996**, *6*, 15-50; b) G. Kresse and J. Hafner, *Phys. Rev. B* **1993**, *47*, 558-561; c) G. Kresse and J. Furthmüller, *Phys. Rev. B* **1996**, *54*, 11169-11186; d) G. Kresse and J. Hafner, *Phys. Rev. B* **1994**, *49*, 14251-14269.

[19] a) P. E. Blöchl, *Phys. Rev. B* **1994**, *50*, 17953-17979; b) G. Kresse and D. Joubert, *Phys. Rev. B* **1999**, *59*, 1758-1775.

[20] J. P. Perdew, K. Burke and M. Ernzerhof, *Phys. Rev. Lett.* **1996**, *77*, 3865-3868.

[21] K. Momma and F. Izumi, *J. Appl. Crystallogr.* **2011**, *44*, 1272-1276.

[22] a) I. Lamparth and A. Hirsch, *J. Chem. Soc., Chem. Commun.* **1994**, 1727-1728; b) I. Lamparth, C. Maichle–Mössmer and A. Hirsch, *Angew. Chem. Int. Ed.* **1995**, *34*, 1607-1609.

[23] C. Bingel, *Chem. Ber.* **1993**, *126*, 1957-1959.

10.1002/chem.201701043

WILEY-VCH

FULL PAPER

We report the synthesis of Ru nanoparticle assemblies with a control of interparticle distances via covalent bonds with functional molecules.

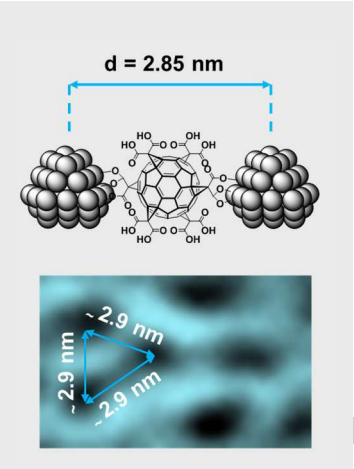

F. Leng, I. C. Gerber, P. Lecante, A. Bentaleb, A. Muñoz, B. M. Illescas, N. Martín,G. Melinte, O. Ersen, H. Martinez, M. R. Axet and P. Serp**

Page No. – Page No.

Hexakis [60]Fullerene Adduct-Mediated Covalent Assembly of Ruthenium Nanoparticles and Their Catalytic Properties